

COPRA EXPERIMENTS ON NATURAL CONVECTION HEAT TRANSFER WITH HIGH RAYLEIGH NUMBERS

Luteng Zhang, Yukun Zhou, Yapei Zhang, Wenxi Tian, Suizheng Qiu, Guanghui Su

Xi'an Jiaotong University

No. 28, Xianning West Road, Xi'an 710049, China

zlt2012@stu.xjtu.edu.cn; zhou.yukun@stu.xjtu.edu.cn; zhangyapei@mail.xjtu.edu.cn;

wxtian@mail.xjtu.edu.cn; szqiu@mail.xjtu.edu.cn; ghsu@mail.xjtu.edu.cn

ABSTRACT

During a severe accident in light water reactors, the melt of the core may relocate into the lower head of the reactor pressure vessel. Natural convection plays an important role in determining the thermal load from the debris pool, which is directly relevant to the problem of retention of molten corium inside the lower plenum. This paper presents the description of COPRA (CORium Pool Research Apparatus) experiments and results on natural convection heat transfer in an internally heated melt pool. The test apparatus is a two-dimensional 1/4 circular slice structure with an inner radius of 2.2 m to simulate the lower plenum of reactor vessel at 1:1 scale for the Chinese advanced PWR. A non-eutectic binary mixture of 20mol% NaNO₃-80mol% KNO₃ compositions is selected as the simulant material. The melt is pre-heated to about 350°C in a custom-designed heating furnace before being transferred to the facility. 20 electrical heating rods, each with a diameter of 16 mm but different lengths according to their locations, are uniformly distributed in the vessel to simulate the homogenous internal decay heat. The top surface of the pool can be maintained insulated with an adiabatic lid. The outside of the curved wall is enclosed with a regulated external cooling path to keep the boundary temperature nearly isothermal. Due to the full scale geometry, the Rayleigh numbers within the pool could reach up to 10¹⁶, matching those in the prototypical situation for PWR. The results have been compared with the correlations from other experiments.

KEYWORDS

Severe accident, IVR, corium pool, natural convection, COPRA

1. INTRODUCTION

During a severe accident in light water reactors, the insufficient cooling capacity may lead to the melt of the core. Furthermore, the corium melt may relocate into the lower plenum of the Reactor Pressure Vessel (RPV) depending on different accident scenarios. The accumulated molten core materials in the lower head could form a hemispherical pool with homogenous internal decay heat, as happened in the Three Mile Island Unit 2 (TMI-2) accident [1]. If there is no effective cooling mechanism, the decay power will gradually heat up the melt pool and then the vessel wall, which will threaten the structural and thermal integrity of the reactor vessel. External Reactor Vessel Cooling (ERVC) is regarded as an effective severe accident mitigation strategy for In-Vessel Retention (IVR) of core melt [2]. The reactor cavity is flooded to submerge the reactor lower plenum in order to cool the melt pool relocated into the vessel lower head. This will create a nearly isothermal boundary outside the vessel wall. The success of ERVC is determined by the heat removal capacity, that is, the heat generated in the melt must balance the energy removed from the pool boundaries to achieve a steady state. Natural convection plays an important role in determining the thermal-hydraulic phenomenon in the debris pool at high Rayleigh numbers, which can be characterized

by buoyancy-induced flows arising from internal decay heating [3]. The convective heat flux distribution depends on many aspects in thermal-hydraulic transient and steady state, such as melt pool configuration, internal power density, adiabatic or cooling boundary conditions, and crust formation.

Some experimental work has been carried out to study the retention of core melt in the lower plenum of the reactor pressure vessel in the past decades. And particular attention was paid to the research of melt thermal hydraulics [4]. Due to different research emphasis and experimental conditions, these experiments were performed in different geometrical facilities with different simulant materials under different boundary conditions, and the melt pool natural convection covers different ranges of Rayleigh numbers [5]. The results of these experiments will be applied to develop models, which can be implemented into severe accident computer codes, such as MAAP, MELCOR and ASTEC.

For the experimental designs of prototypical corium pool simulation, the approximation of the internal Rayleigh number Ra' ($Ra' = g\beta q_c H^5 / \lambda \nu \alpha$) is the most important consideration. It should be noted that the pool height H determines Ra' at the power of 5. Many experiments were conducted in large-scale 2D slice facilities to respect the internal Rayleigh number, such as COPO [6] and BALI [7] experiments, as well as the large scale ACOPO-3D experiments [8]. Based on this research direction, COPRA experiments are performed to study the natural convection heat transfer in corium pools with high Rayleigh numbers.

2. EXPERIMENTAL SETUP

2.1. Facility Description

The COPRA (CORium Pool Research Apparatus) test facility is a two-dimensional 1/4 circular slice structure comprised of the test vessel, cooling path and upper lid, as shown in Fig. 1.

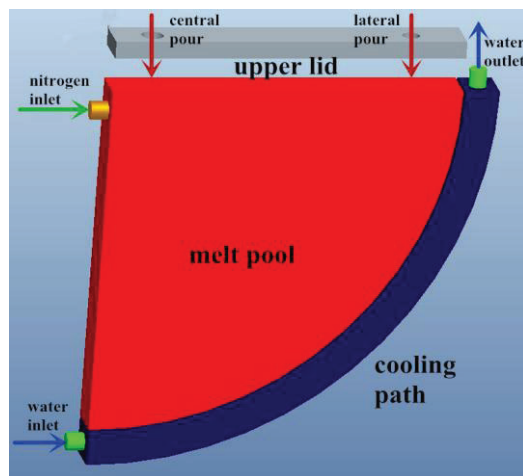


Figure 1. Diagram of the COPRA test facility

The test vessel has an inner radius of 2.2 m to simulate the lower plenum of reactor vessel for the Chinese advanced PWR at 1:1 scale. The inner width of the slice is 20 cm. All the vertical walls of the vessel have the thickness of 25 mm and are kept thermally insulated. The curved vessel wall has the thickness of 30 mm and was enclosed from outside with a regulated external cooling path to keep the boundary temperature nearly isothermal. The cooling water inlet and outlet are located at the bottom and top of the vessel respectively. The top surface of the vessel has the adiabatic boundary condition with the insulated upper lid. Two openings are designed in the insulated lid to allow melt pouring position either near centre

or close to the perimeter of the vessel wall, at polar angle of 65° . This design is aimed to study the influence of the relocation position of heat transfer characteristics. Due to the full scale geometry, the modified Rayleigh numbers within the pool could reach up to 10^{16} , matching those in the prototypical situation for PWR.

A non-eutectic binary mixture of 20%NaNO₃-80%KNO₃ (mole fraction) compositions is selected as the simulant material. The temperature gap between the solidus (225°C) and liquidus (284°C) temperatures for this mixture could reach to about 60°C. Therefore this kind of molten material can be used in a temperature range between 225°C (solidification) and 380°C (chemical decomposition) [9]. In addition, with this simulant material, a similar solidification behavior could occur as the prototypical corium due to the characteristics of multi-component and distinctive solidus-liquidus temperature gap. More detailed information about properties of NaNO₃-KNO₃ mixture is available in literature [10-12]. When scaling to the prototypical reactor case, in the most conservative situation with 100% anticipated melting of the whole core inventory including both oxidic and metallic components, the surface of the melt pool could reach to the polar angle of 75° - 82° [1, 13]. Therefore, the melt pool inside the COPRA facility could reach to the height of 1900 mm with the volume about 0.6 m³. The melt is pre-heated to about 350°C in a custom-designed heating furnace before being pumped to the test vessel through the openings in the upper lid.

20 electrical heating rods, each with a diameter of 16 mm but different lengths, are horizontally distributed in the vessel to simulate the decay heat. They can provide a maximum of 30 kW power to the melt pool. The heating rods are divided into ten groups according to their installation height, thus dividing the melt pool into ten heating zones. Based on the corresponding volume of each heating zone, homogenous internal heating could be achieved by adjusting the heating power of each group. Table I presents the parameters of the heating rods and heating zones. The internal Rayleigh numbers could reach to about 1.3×10^{16} with the heating powers of 10 kW.

Table I. Details of the heating rods and heating zones

Zone NO.	Rod height /mm	Rod length /mm	Zone volume /L	Volume fraction	Heating power /W	Power density /W·m ⁻³
1	95	300	22.86	0.036	363.64	15906.65
2	285	920	40.93	0.065	651.06	15906.65
3	475	1240	51.78	0.082	823.59	15906.65
4	665	1470	59.82	0.095	951.46	15906.65
5	855	1660	66.10	0.105	1051.44	15906.65
6	1045	1800	71.11	0.113	1131.09	15906.65
7	1235	1910	75.09	0.119	1194.47	15906.65
8	1425	2000	78.21	0.124	1244.05	15906.65
9	1615	2060	80.56	0.128	1281.46	15906.65
10	1805	2100	82.21	0.131	1307.75	15906.65
Total			628.67	1	10000	15906.65

79 K-type thermocouples (PT) are installed in the melt pool to measure the melt pool temperature field. 24 pairs of T-type thermocouples (IT/OT) are located inside the curved wall at the positions 3 mm departure from the inner and outer surface of the curved wall. IT/OT measuring points are designed on both front and back sides of the vessel to ensure the effectiveness of local heat flux distribution along the

curved wall. In the cooling path, 3 T-type thermocouples are located at polar angles of 0° , 45° , and 90° to monitor the change of water temperature. Moreover, 6 multipoint thermocouples (CT), each with seven measuring points, are installed along the inside vessel wall to quantify the characteristics of crust behavior. Table II presents the parameters of the multipoint thermocouples. The locations of the heating rods and thermocouples are presented in Fig. 2.

Table II. Details of the multipoint thermocouples

NO.	Polar angle	Distances of measure points from the inside wall/mm
1	10°	5、 15、 25、 40、 55、 65、 75
2	20°	
3	30°	
4	40°	5、 15、 30、 45、 50、 55、 60
5	50°	5、 15、 20、 25、 30、 35、 40
6	60°	

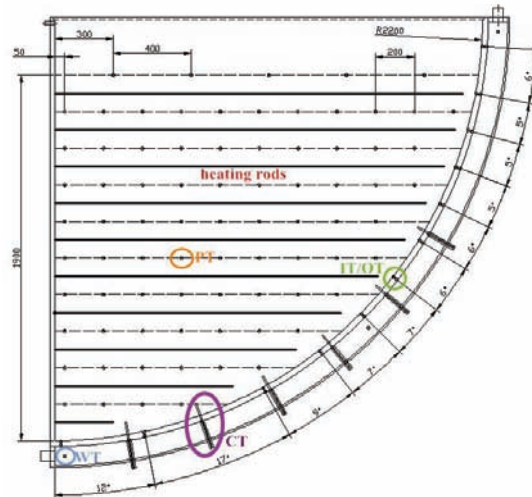


Figure 2. Locations of heaters and the rmocouples

The schematic diagram of the experimental loop is depicted in Fig. 3. The loop consists of test section, heating furnace, and circulating cooling water system. During the process of heating and pouring, the melt was protected by nitrogen to avoid the possible change of melt composition and properties in the circumstance of high temperature and air atmosphere. At the same time of melt pouring, the electrical heating rods were fixed to the designed voltages and powers to produce nearly homogenous heating. The outside surface of the curved wall was cooled by water with a flow rate of about 5 kg/s. The temperature fluctuation along the curved wall outer surface could be maintained within $\pm 1^\circ\text{C}$, thus creating the nearly isothermal boundary condition. The cooling water carried the heat from melt pool to the heat exchanger and was cooled then by the cooling tower to the inlet temperature. The steady state of the melt pool was reached when the internal heating power balanced the heat removed from the curved wall. After the test, the melt in the slice pool was discharged through the opening at the bottom of the vessel to the drain tank. During the experiment, all the measured heating powers, temperatures and water flow rates were real-time monitored in the data acquisition system (DAS).

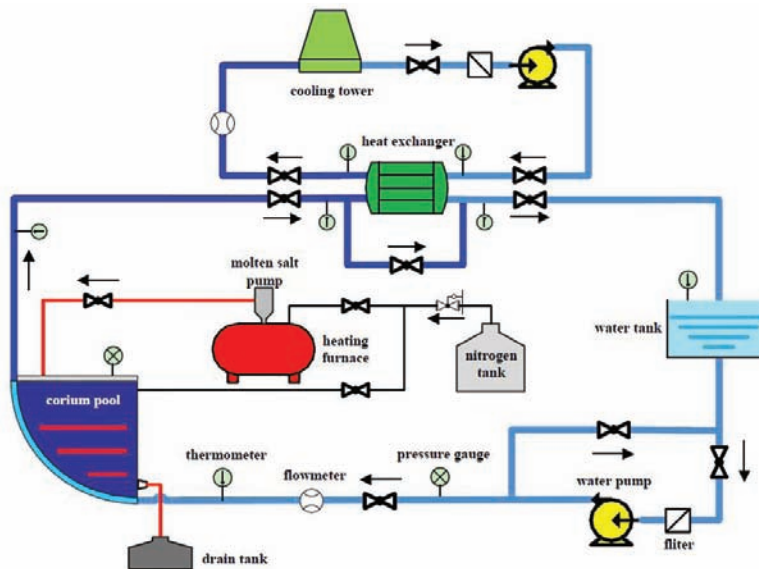


Figure 3. Schematic diagram of the COPRA experimental loop

2.2. Test Matrix

The COPRA experiments are designed to study the heat transfer phenomenon in corium pools with high Raleigh numbers. As shown in Table III, four tests have been performed to study the influence of relocation position, pool height and power density on pool temperature field and heat flux distribution, as well as the crust formation along the inner curved wall. The range of Ra' of COPRA experiments lies between 1.188×10^{15} and 1.784×10^{16} .

Table III. COPRA test matrix

Test NO.	Relocation position	Pool height/mm	Pool volume/m ³	Heating power/kW
1	lateral	1900	0.629	8
2	lateral	1900	0.629	15-10-15
3	central	1140	0.313	10-7-12-14
4	stage 1	central	1140	14
	stage 2	central	1900	15-10-15

In the first three tests, melt was pumped into the vessel at one time from different relocation positions with different internal heating powers. While in the fourth test, melt was poured in two times. After the first release of 0.313 m³ melt reached to its steady state with 14 kW heating power, second release was performed. And the melt pool height was then elevated from 1140 mm to 1900 mm. All the steady states were lasted for at least one hour for data processing.

3. RESULTS AND DISCUSSION

3.1. Pool Temperature

Fig. 4 shows the transient pool temperature evolution after the melt relocation in test 1. It can be seen that the initial melt temperature was about 325°C and gradually decreased and reached to its steady state at 285°C. The duration of relocation process was about 2 minutes.

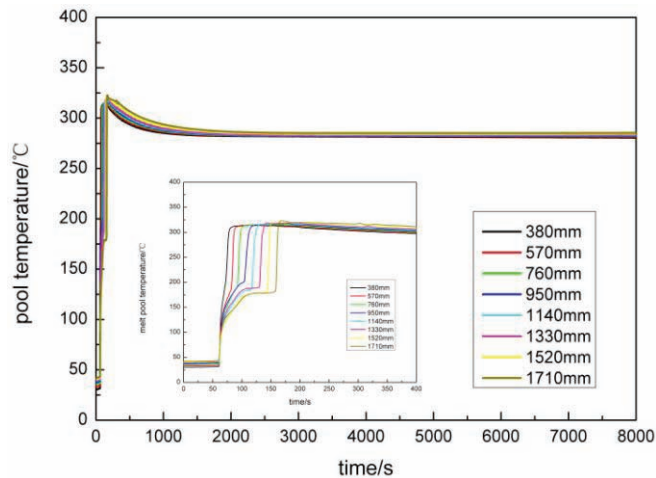


Figure 4. Melt pool temperature evolution after relocation in test 1

The averaged temperature distributions along pool heights in the test 2 steady states are illustrated in Fig. 5. It clearly shows that thermal stratification occurred in the steady states with higher temperatures and lower temperature gradients in the upper part. The temperature field in the middle and upper pool in phase 1 and 3 were similar with the same heating power, both higher than those in the phase 2 with smaller heating power. However, in the phase 3, the averaged temperatures at the heights lower than 600 mm were obviously lower than phase 1 because some part of the lower pool was already merged in the crust part. When normalizing the pool temperature at different heights over the averaged pool temperature, as shown in Fig. 6, the temperature distribution shows good similarity with each other, regardless of heating powers. Therefore the experimental results could be extrapolated to situation with higher power density.

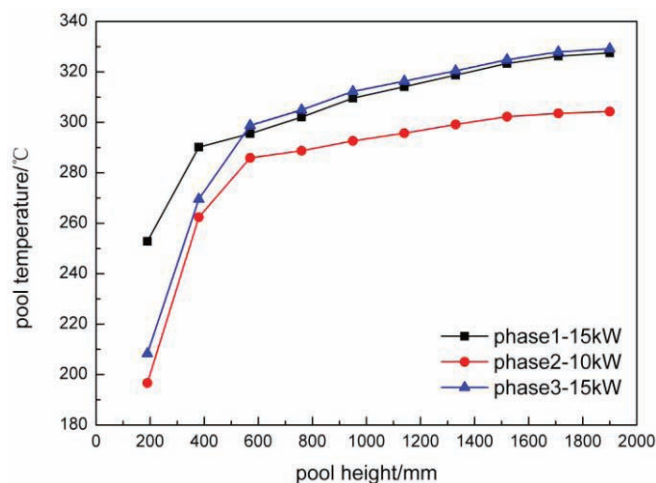


Figure 5. Melt pool temperature distribution in steady states in test 2

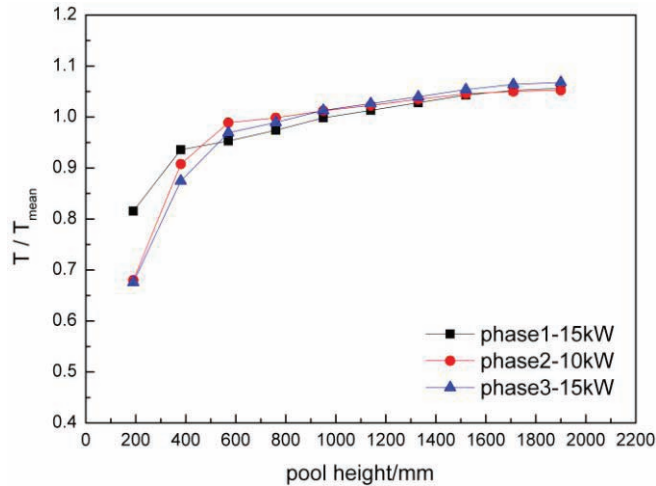


Figure 6. Normalized melt pool temperature distribution in test 2

Fig. 7 presents the pool temperature evolution during the process of second relocation in test 4. A sudden increase of temperature was observed in the upper part when the melt was pumped in and the whole melt pool gradually reduced to its new steady state. It needs less time to reach to the new steady state compared to the first relocation. Influences of heating power transitions on melt pool temperature are shown in Fig. 8. It can be seen that the melt at the bottom responded more quickly to the power transition. More time was needed for the upper part to reach the steady state. Three reasons contribute to this phenomenon: 1) smaller volume of the lower part of melt pool needs less time to respond; 2) the melt bulk in the top is farther from the cooling water than that in the bottom; 3) heat transfers to upside more easily than sideward and downward.

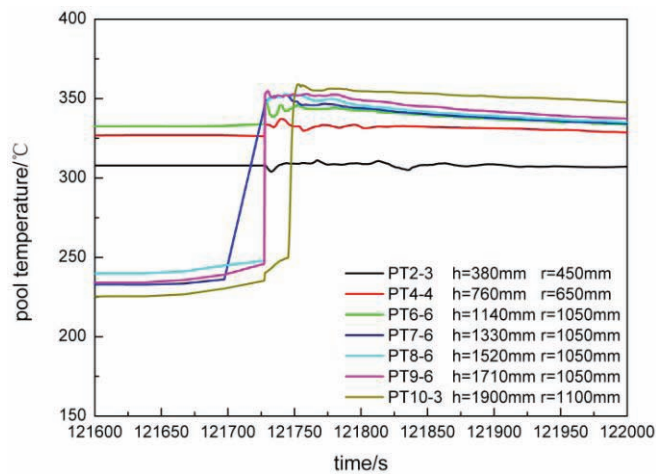


Figure 7. Melt pool temperature evolution after 2nd relocation in test 4

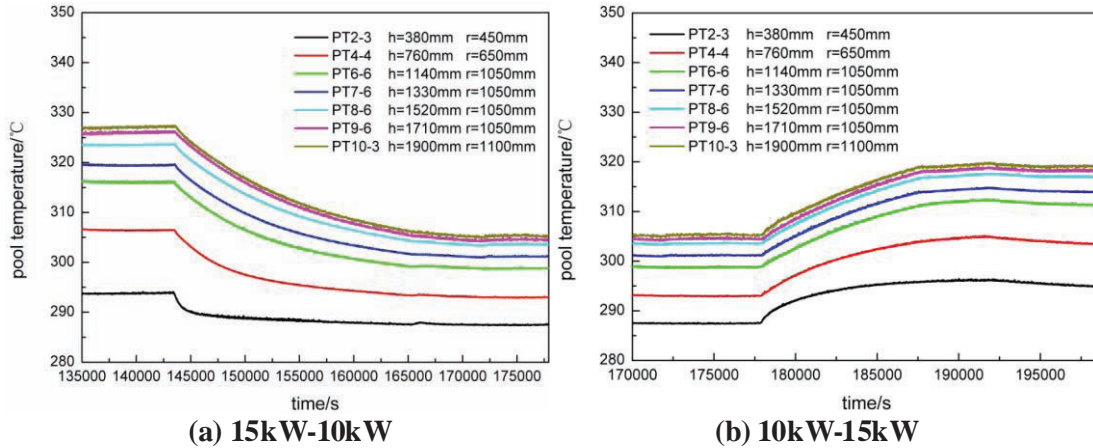


Figure 8. Melt pool temperature evolution during power transition in test 4

3.2. Heat Transfer

The local heat flux distribution and its normalized values along the curved wall in the test 2 are illustrated in Fig. 9 and 10, respectively. Heat transfer below polar angle of 40° appeared to be flat, and obvious increase of heat flux occurred from 40° up to the pool surface. The maximum heat flux occurred in the upper part slightly lower than the pool surface. The radiation heat transfer from the free melt surface to the upper atmosphere led to the decrease in heat transfer to the side wall at the top. Apparently, larger heating power led to higher temperatures and heat fluxes, but it was not obvious in the lower part of the pool. The values of heat flux in the phase 3 were slightly lower than those in the phase 1 due to the thicker crust formation than the initial stage. When normalizing the local heat transfer over the averaged value, the results presented good similarity among the three phases in the lower and middle part of the pool. Much higher q_{local}/q_{mean} ratio was reached in the phase 3 than phase 2, with a value about 2.6. Smaller ratio was found in the phase 2 because of the smaller heating power and thicker crust. Similar heat transfer distribution characteristics were found in the test 3 and 4.

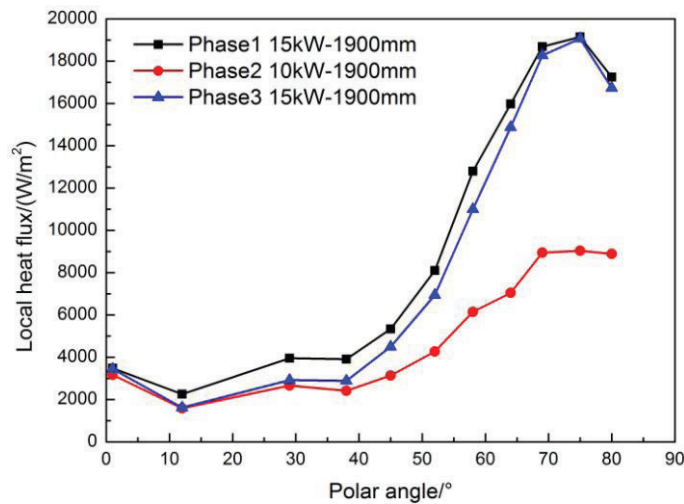


Figure 9. Local heat flux distribution in test 2

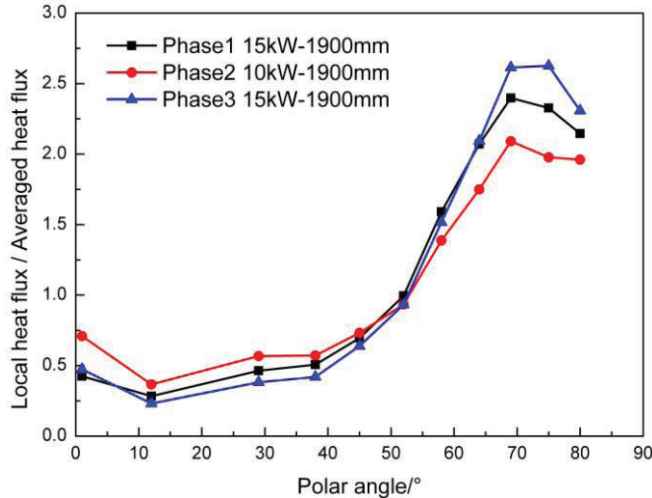


Figure 10. Normalized heat transfer distribution in test 2

Comparison between test 2 and test 4 showed that the relocation positions from centre or lateral influenced the final heat flux distribution. The melt from non-central pouring would flow to the bottom along the cold side wall, which would create a thicker crust layer than those in the situation from central pouring. This will lead to lower heat transfer at bottom and higher q_{local}/q_{mean} ratio at top, as shown in Fig. 11. It indicates that the melt injection process in the initial transient stage could influence the heat flux distribution in the steady state of the molten pool. Therefore the central relocation position can weaken the thermal shock on the lower head wall in the long-term cooling process of RPV.

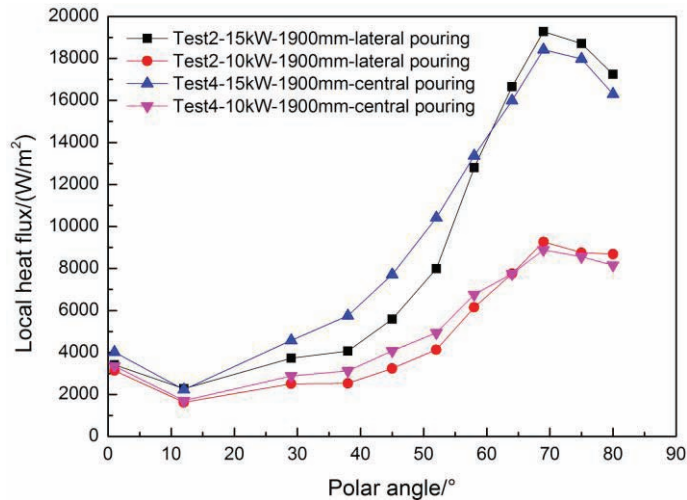


Figure 11. Influence of relocation position on heat flux

3.3. Crust Formation

Fig. 12 presents the crust thickness evolution during the test period. The crust layer was formed immediately when the melt contacted with the cold vessel wall. Then the crust gradually grew thicker until the vessel wall was heated to certain temperature. Then the internal heat began to melt some part of the crust to reach the steady state. When the heating power was changed to 7 kW, an obvious increase of

crust thickness was observed. A sudden increase of crust thickness was found at polar angle of 40° when increasing the heating power to 12 kW. It indicated that more times of heating power transition may facilitate crust cracking and lead to the penetrating of hot melt into the crust interface. As a result, the crust became thicker after the events [13]. The distribution characteristics of crust thickness in steady states are shown in Fig. 13. The crust becomes thinner with increasing polar angles due to the higher heat flux in the upper part.

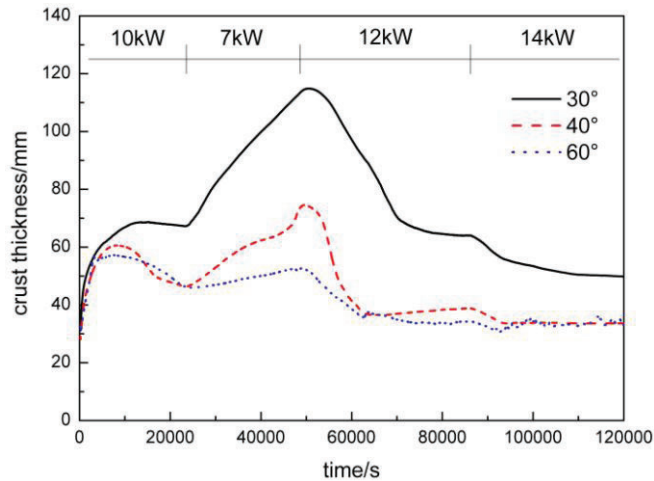


Figure 12. Crust thickness evolution in test 3

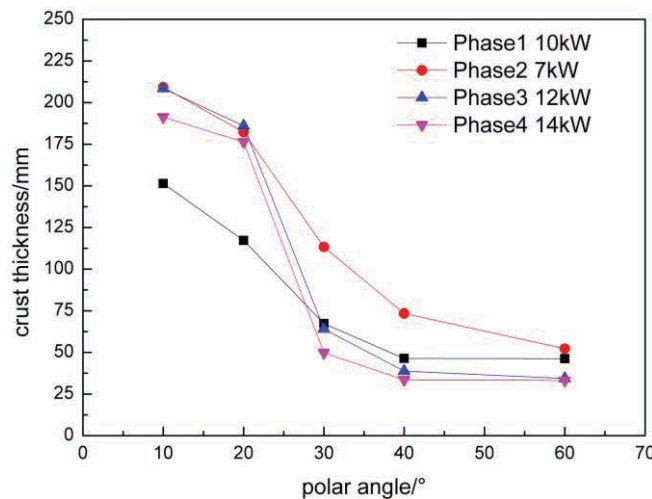


Figure 13. Crust thickness distribution in steady states in test 3

3.4. Comparison with Other Experiments

Downward heat transfer in COPRA experiments are compared with previous experimental results and relations in Fig. 14. Most of the previous experiments are in the Ra' region lower than 10^{14} , such as SIMECO [14] and LIVE [15] experiments. It can be seen that the downward heat transfer Nu_{dn} increases with larger Ra' , and the results from COPRA are lower than those from ACOPO [1] and BALI [7] predictions. It should be noted that there was no internal heating in the ACOPO experiments. Therefore, the internal heating in the COPRA experiments would drive more heat to the upper surface through

natural convection, leading to lower heat transfer along the curved wall. For the BALI experiments, the ice was formed in the BALI water simulation experiments. The ice has higher conductivity and lower porosity compared to the salt crust in the COPRA. As a result, the higher crust thermal resistance in the COPRA experiments caused lower heat transfer towards the curved wall. More importantly, compared to the rigid upper boundary condition in the ACOPO and BALI experiments, radiation heat loss from the free top surface in the COPRA melt pool would lead to lower heat transfer to the downward curved wall.

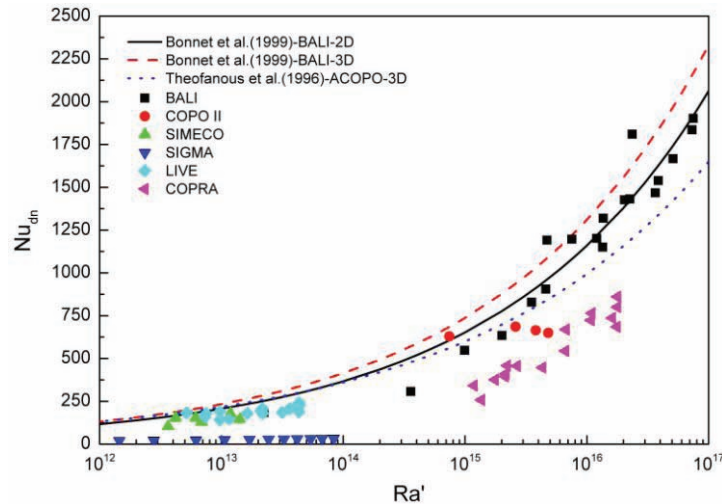


Figure 14. Downward Nu comparison with other experiments

4. CONCLUSIONS

The COPRA experiments are performed to study the natural convection heat transfer in corium pools with high Rayleigh numbers. The influence of relocation position, pool height and power density on pool temperature field and heat flux distribution, as well as the crust formation along the inner curved wall are studied. The Rayleigh numbers could reach to $1.188 \times 10^{15} \sim 1.784 \times 10^{16}$ to cover the prototypic range of Rayleigh numbers of current interest of in-vessel retention.

Thermal stratification occurred in the steady states of melt pool with higher temperatures and lower temperature gradients in the upper part. The melt at the bottom responds more quickly to the power transition. More time is needed for the upper part to reach the steady state. Normalized melt pool temperature distribution shows good similarity with each other, regardless of heating powers.

Heat transfer along the curved wall below polar angle of 40° appeared to be flat and obvious increase of heat flux occurred from 40° up to the pool surface. The maximum heat transfer occurs in the upper part near the pool surface. The maximum q_{local}/q_{mean} ratio could reach up to about 2.6.

The crust becomes thinner with increasing polar angles. More times of heating power transition may facilitate crust cracking and create thicker crust. Non-central pouring will form thicker crust layer at vessel bottom and lead to larger q_{local}/q_{mean} ratio at the top of the melt pool.

It can be seen that the downward heat transfer Nu_{dn} increases with larger Ra' . Comparison with previous experiments shows that the downward heat transfer Nu_{dn} from COPRA experiments are lower than those from ACOPO and BALI predictions.

REFERENCES

1. Theofanous, T.G., et al., In-vessel coolability and retention of a core melt. *Nuclear Engineering and Design*, 1997. 169(1-3): p. 1-48.
2. Zhang, Y.P., et al., A simple novel and fast computational model for the LIVE-L4. *Progress in Nuclear Energy*, 2013. 68: p. 20-30.
3. Lee, S.D., J.K. Lee, and K.Y. Suh, Natural convection thermo fluid dynamics in a volumetrically heated rectangular pool. *Nuclear Engineering and Design*, 2007. 237(5): p. 473-483.
4. Asmolov, V., et al., Challenges left in the area of in-vessel melt retention. *Nuclear Engineering and Design*, 2001. 209(1-3): p. 87-96.
5. Zhang, L., et al., Natural convection heat transfer in corium pools: A review work of experimental studies. *Progress in Nuclear Energy*, 2015. 79(0): p. 167-181.
6. Kymäläinen, O., H. Tuomisto, and T. Theofanous, In-vessel retention of corium at the Loviisa plant. *Nuclear Engineering and Design*, 1997. 169(1): p. 109-130.
7. Bonnet, J.M. and J.M. Seiler. Thermal hydraulic phenomena in corium pools: the BALI experiment. in 7th International Conference on Nuclear Engineering (ICONE). 1999. Tokyo, Japan.
8. Theofanous, T.G., et al., The first results from the ACOPO experiment. *Nuclear Engineering and Design*, 1997. 169(1-3): p. 49-57.
9. Miassoedov, A., et al., Results of the Live-L4 Experiment on Melt Behavior in the Rpv Lower Head. *Proceedings of the 18th International Conference on Nuclear Engineering 2010*, Vol3, 2011: p. 475-482.
10. Zhang, X.J., et al., Thermodynamic evaluation of phase equilibria in NaNO₃-KNO₃ system. *Journal of Phase Equilibria*, 2003. 24(5): p. 441-446.
11. Berg, R.W. and D.H. Kerridge, The NaNO₃/KNO₃ system: the position of the solidus and sub-solidus. *Dalton Transactions*, 2004(15): p. 2224-2229.
12. Janz, G.J., et al., Physical properties data compilations relevant to energy storage-II. Molten salts: Data on single and multi-component salt systems. *NASA STI/Recon Technical Report N*, 1979. 80: p. 10643.
13. Gaus-Liu, X., et al., Test and Simulation Results of LIVE-L4+ LIVE-L5L. Vol. 7593. 2011: KIT Scientific Publishing.
14. Sehgal, B.R., et al. SIMECO Experiments on In-Vessel Melt Pool Formation and Heat Transfer with and without a Metallic Layer. in *Proc. OECD/CSNI Workshop*. 1998. Garching, Germany.
15. Gaus-Liu, X. and A. Miassoedov. Live Experimental Results of Melt Pool Behaviour in the PWR Lower Head With Insulated Upper Lid and External Cooling. in *2013 21st International Conference on Nuclear Engineering*. 2013. American Society of Mechanical Engineers.